ISSN (Online) 2620-7222
ISSN (Print) 2503-2399

Available online at
https://jurnalteknik.unisla.ac.id/index.php/CVL

https://doi.org/10.30736/cvl.v2i2

Experimental and Confining Pressure Analysis of Steel Clamp Confined Unreinforced Concrete Subjected to Axial Concentric Load

Sandy I. Yansiku[1*], Jimmy Chandra[2]
[1*],*Department of Engineering Profession, Atma Jaya Catholic University of Indonesia,*
[2]*Civil Engineering Department, Petra Christian University*
Email : [1*] sandyyansiku@gmail.com. [2]chandra.jimmy@petra.ac.id.

A R T I C L E I N F O

Article History :
Article entry : 25-06-2025
Article revised : 02-07-2025
Article received : 26-09-2025

Keywords :
External Retrofitting, Steel Clamp, Confining Pressure, Strength, Ductility.

IEEE Style in citing this article :
S. I. Yansiku and J. Chandra, "Experimental and Confining Pressure Analysis of Steel Clamp Confined Unreinforced Concrete Subjected to Axial Concentric Load", CVL, vol. 10, no. 2, pp. 187–199, Sep. 2025.

A B S T R A C T

Vertical cracks and spalling of the concrete cover in reinforced concrete structures are examples of failure modes of concrete columns due to repeated earthquake loads. Strengthening methods have been introduced including external jacketing using costly carbon FRP. This study investigated external strengthening of cylindrical concrete using low-cost thin steel confining sheets subjected to concentric axial loads. The experimental works in this study tested the tensile strength of the confining steel elements, the compressive strength of unconfined and confined cylindrical concrete. The composition of the steel confining elements is positioned in such that it could generate an optimal confinement effect and prevent local buckling. This study also developed the formulation of the confining stress and ultimate axial load based on the test results of the current study and past research data. The results showed that the use of steel clamp elements improves the axial strength and axial deformation of cylindrical concrete columns by over 200% without buckling of the clamp elements. The external confinement method can reduce vertical cracks and strain localization that usually occur in conventional cylindrical concrete. The proposed formulation of the confining stress and the ultimate axial load provided accurate results compared to the experimental results.

1. Introduction

Scientific research concerning the internal and external confinement of concrete columns has been developed for decades. Additional strengthening methods are often required to satisfy the lateral performance demand of structure in highly seismic intensity region [1]. External retrofitting methods of concrete columns include CFST (Concrete Filled Steel Tube) and STCC (Steel Tube Confined Concrete). Both methods serve a similar purpose but differ in terms of the loading application. In the CFST method, the axial loading is applied to the concrete and the confining steel cover, whereas in STCC, the loading is only carried by the

ISSN (Online) 2620-7222
ISSN (Print) 2503-2399

concrete column. The STCC confinement method can be full confinement or partial confinement. Partial confinement is considered to generate advantages in limiting buckling in the confinement plate that often occurs in CFST. In various research references, the procedure for implementing the testing of reinforced concrete columns using the STCC method is generally outlined for publication interests and requirements. Steel Tube Confined Concrete (STCC) as one of the external concrete retrofitting methods is believed to be able to increase the axial bearing capacity of concrete columns and increase column ductility in addition to limiting the buckling of the confining elements during loading. The relevant studies about STCC refer to the publication of [2], and one of the studies on concrete reinforcement with a steel clamp has been conducted [3] as depicted in Figure 1. When the concrete column experiences uniaxial compression loading, the column deforms vertically and horizontally. Axial deformation of the concrete not only causes changes in the height of the concrete but also causes horizontal/lateral deformation in the segment around the middle of the column span. This deformation occurs due to the localization of strain in the segment triggering the formation of shear bands [4]. The localization often occurs in concrete with the addition of [5], [6], [7] waste material. The formation pushes the volume composition of the concrete in the middle of the span expanding towards the surface. The expansion is followed by separation or dilation of the concrete cover as an early indication of the collapse of the column element. To prevent this separation, the column element needs to be laterally strengthened to limit and prevent failure as indicated in Figure 2. Researches into externally steel-confined concrete have been extensively conducted [8], [9], [10], [11], [12], [13], [14], [15], [16], [17].

Experimental and analysis studies excluded the initial stress distribution by confining pressure of clamps towards the column surface and the frictional stress within the interface between clamps and concrete surface. The initial tightening stress to each clamping unit should be evenly applied to maintain the balancing stress to the surface. The friction stress within the interface should be avoided because the movement of the clamps may reduce the overall measured confining pressure. In previous studies on slender reinforced concrete columns [18], [19], the numerical work revealed that the initial and frictional stresses generated a minor effect on the total confining pressure under higher concrete compressive strength levels. The effect was graphically visible on the early loading application of all included parametric factors. This study aims to provide an adequate experimental description and in-depth analysis of the implementation of the normal strength concrete columns that are externally strengthened by steel clamps under uniaxial concentric compression. The experimental work takes into account the balancing stress distribution on the initial clamping pressure and the analysis includes the frictional stress to obtain the theoretical total confining pressure in retrofitting the unreinforced concrete specimen. The analysis formulates the stress-strain model for the specific cases of this study.

Source : (Holmes et al., 2015).[3]
Figure 1. Column Specimen Retrofitting with Steel Clamp.

ISSN (Online) 2620-7222
ISSN (Print) 2503-2399

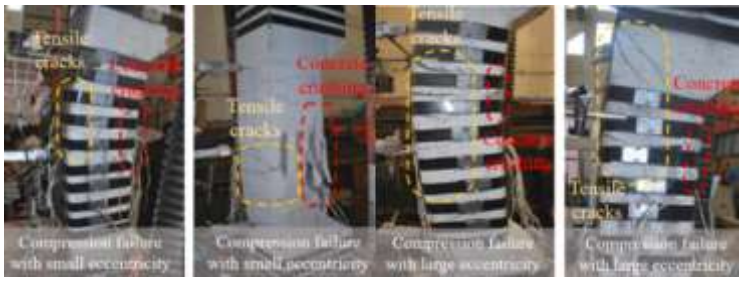

Source : (Chen et al., 2022).[8]
Figure 2. Purpose of Externally Confined Concrete with Steel Strips.

2. Research Method

This study involves an experimental and analytical approach to achieve the objectives of this study. Firstly, two experimental works are conducted to test the properties of steel and concrete materials. Then, the analytical method is utilized to derive the formulation based on previous studies and test results. The experimental test uses a cylindrical unreinforced concrete column with a diameter D of 110 mm and a height H of 200 mm. Two specimens of an unconfined concrete column, as the reference specimen, and the externally confined concrete column using steel clamps. The mix design of the normal-strength concrete follows the common mix design standard in Indonesia, SNI 03-2834-2000 [20]. The width of the steel confining unit h_s is 25 mm and the thickness t_s is 1 mm with the maximum clamping diameter of 120 mm as indicated in Figure 3. The diameter of the clamp is larger than the diameter of the concrete cylinder specimen to facilitate the installation of the clamp on the concrete cylinder. In this test, one concrete specimen is strengthened with 5 clamp units by maintaining a similar gap g_s of 17.5 mm. The clear distance between the top-most clamp unit and the top edge of the column is 2.5 mm. Hence, only the concrete surface is subjected to axial compression. Similar treatment was applied to the bottom edge of the column. To determine the capacity of the steel clamp and its tensile characteristics, a coupon test (uniaxial tensile test) is carried out based on the SNI-07-0408-1989 standard. The size of the coupon is shown in Figure 4.

Source : (Experimental works, 2025).
Figure 3. Steel Clamp.

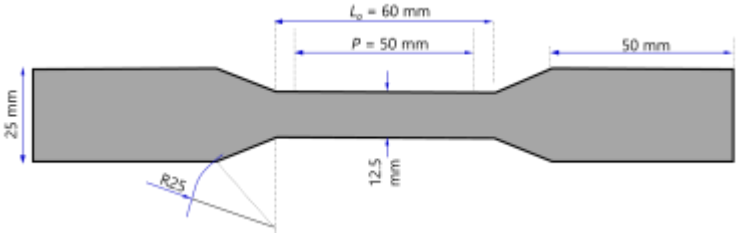

Source : (Experimental works, 2025).
Figure 4. Coupon Tensile Test of Steel Sheet.

ISSN (Online) 2620-7222
ISSN (Print) 2503-2399

2. Testing Instruments and Description

Several test tools are utilized to obtain the appropriate output. In large-scale testing with a large number of measuring instruments, the accuracy in use, input, and correct installation are the key factors in obtaining accurate test data results. In this test, the measurement of test parameters (axial load, vertical and horizontal displacement, strain) uses a load cell, linear variable differential transformer (LVDT), and strain gauge (SG), respectively. Applied axial load was measured using a 100 MN load cell, whereas the vertical and horizontal displacements were measured using two LVDTs. In this test, two LVDTs measure the vertical and the horizontal deformation of a concrete cylinder subjected to axial compression. The vertical LVDT is placed on the load plate under the load cell distributed on the entire surface of the concrete specimen, while the horizontal LVDT is placed on the surface of the concrete cylinder right in the middle height of the concrete (z =100 mm).

Three strain gauges were utilized to measure the strain of the middle unit of steel clamps. A tester is used to measure the amount of resistance in Ohms of the strain gauges. After the strain gauge is attached to the concrete or steel element, it is required to ensure that the installation is correct and the strain gauge continues to function normally after gluing [21]. The induction between the two fiber poles (+/-) of the copper strain gauge due to gluing or clamping should be avoided. The amount of resistance in the strain gauge specifications used is 118.5±0.5 **Ω**.

Source : (Experimental works, 2025).

Figure 5. Instrumentation of Confined Concrete Test.

The measurement on the tester is 0.120 using a 2K scale (2000 **Ω**) indicating that the resistance is 120 **Ω**, slightly higher than the resistance range in the product specification. This difference is caused by measuring the resistance immediately after the gluing process so that the temperature of the adhesive still affects the measurement. In this test, axial loading is applied by displacement control on the upper loading plate of the UTM. The control panel will regulate the displacement speed (load rate) and record the amount of vertical displacement (mm) and the load required (kgf) to compress the concrete specimen. For strain measurement, one strain gauge unit (SGc) is placed on the concrete and another unit (SGs) is mounted on the steel clamp number 3 as shown in Figure 5. Each measuring device is connected to a data logger. For the accuracy of deformation measurements, two LVDT units are utilized to measure vertical displacements in line with the displacement control of the testing machine and horizontal displacements of the composite specimen. Figure 5 illustrates the instrumentation of the specimen within the testing machine.

ISSN (Online) 2620-7222
ISSN (Print) 2503-2399

3. Results and Discussions

3.1 Tensile Test Results of Steel Clamp

The tensile strength test of 3 thin steel plate specimens begins with the provision of a tensile load in the form of displacement control at a speed of 0.16 mm/second by the UTM until the plates fail due to tensile force. In this test, the plate failed at the average tensile load of 335.41 kgf with a maximum deformation of 37.84 mm in 2 minutes. The raw output of the UTM testing machine is in the form of displacement, tensile load and duration of the test. The records of the mechanical characteristics of the steel plate from the test results is then processed to obtain the average tensile strength according to the desired units. Calculations are carried out to determine other parameters as presented in Table 1. The value of the elastic modulus of steel is assumed to be 200 GPa to obtain the yield strain and ultimate strain using conventional formulations $\varepsilon_y = E_s f_y$ and $\varepsilon_{s-ult} = E_s f_{y-ult}$. The results of the tensile tests show the average ultimate tensile strength of 258 MPa and the average yield strength of 181 MPa.

Table 1. Mechanical Properties of Thin Steel Plates from Test Results

Specimen	t_s mm	h_s mm	L_o mm	A_s mm^2	P_y N	P_u N	f_y MPa	f_u MPa	e_y	e_u
1	1.02	12.5	50	12.8	2301.4	3287.8	180.5	257.9	9.03E-4	0.00129
2					2306.6	3295.1	180.9	258.4	9.04E-4	0.00129
3					2299.4	3284.8	181.2	258.9	9.06E-4	0.00129
Average					2302.5	3289.2	180.9	258.4	9.04E-4	0.00129

Source : Test results (2025).

The displacement versus force curve obtained from the testing machine was converted into the tensile stress-strain curve. The load-displacement curve obtained from the test were refined before being used in the analysis. The refinement extends the straight/elastic segment until it intersects the displacement axis in Figure 6. The abscissa of the intersection is the quantity used in shifting the refined curve to point (0,0). If the yield stress is assumed to be 80% of the ultimate stress, the yield point in the figure can be determined. Furthermore, adjustments are made to other segments with the actual yield point and the ultimate point on the final curve.

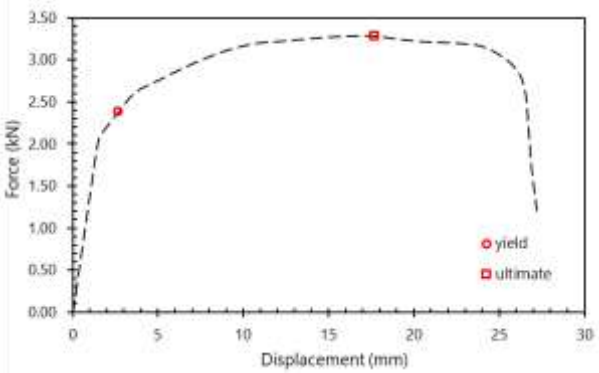

Source : (Experimental works, 2025).
Figure 6. Tensile Test Curve.

3.2. Test Results for the Unconfined Compressive Specimen

An unconfined concrete specimen was tested to measure its concentric axial bearing capacity due to the strengthening mechanism and to obtain the type of failure and cracking in concrete. The axial loading by displacement control in this test was at a speed of 0.2 mm/min until the concrete failed. Figure 7 shows the failure pattern of the concrete at the ultimate compressive load of 10367.6 kgf, the vertical displacement of 3.04 mm after 18 minutes of

ISSN (Online) 2620-7222
ISSN (Print) 2503-2399

load applications. Based on observations, the unreinforced concrete specimen experienced vertical cracks in the direction of axial loading as reported [22], and the concrete cover spalled off due to the strain localization at the middle segment. Setting time during concrete curing is

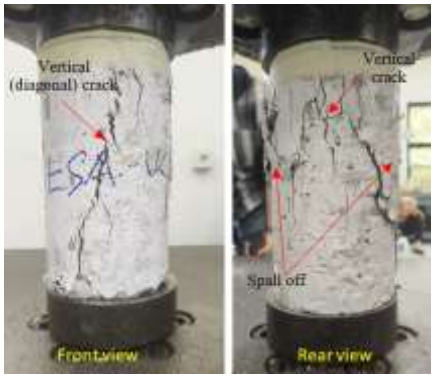

Source : (Experimental works, 2025).
Figure 7. Failure Pattern of Unconfined Concrete Specimen.

essential to obtain optimum compressive strength [23]. The strain localization forms shear bands as the trigger for initial cracks. The peak load of 101.67 kN generates the compressive strength of 10.7 MPa.

3.3. Test Results for the Confined Compressive Specimen

With a similar load rate of 0.2 mm/second, the vertical movement of the load plate of the testing machine axially pushes the load cell and is transmitted to the surface of the confined concrete specimen. As a result of the loading, the concrete specimen experiences a strain localization that reaches an optimum value at the middle segment of the column span leading to a lateral deformation of the concrete at this segment. When there are interactions between the concrete surface and the steel plate due to the lateral deformation of the concrete and the difference in Poisson's ratio between concrete and steel, the active confinement starts. The steel plate attempts to restrain the lateral deformation of the concrete to its ultimate tensile strength. If the vertical load is continuously intensified in such that the stress due to the lateral deformation of the concrete exceeds the tensile strength of a steel plate, the steel clamp fails and the overall confinement process is considered to be terminated, and the concrete is crushed, as shown in Figure 8. The reading on the testing machine showed the maximum load of 24618.1 kgf (241.4 kN) at a vertical displacement of 15.53 mm. After the peak load, the displacement control block was continuously increased until the maximum displacement reached 36.14 mm. The difference in the number of readings between the data logger (2732 points) and the UTM (2360 points) led to a difference in the abscissa range, which may generate errors in strain interpretation.

Considering the advantages of sensitivity and measurement accuracy of the loadcell compared to the UTM, the loadcell loading data was used with the ultimate load of the testing machine as the reference. The displacement and strain versus axial load in Figure 9 improve the reliability of the plots for stress analysis on the test specimen. The strain of the concrete and steel clamp was plotted in Figure 9(a), the vertical and horizontal displacement of concrete were plotted in Figure 9(b), whereas the stress-strain comparison of unconfined and confined specimens was plotted in Figure 9(c). It is seen that the maximum axial load of strain and displacement is identical. In contrast, the vertical and lateral behavior of concrete differs significantly due to the difference in Poisson's effect in both directions of the specimen. In Figure 9(c), the confinement effect of the steel clamps shows remarkable stress and strain improvement. The axial stress of the unconfined specimen was 10.7 MPa and is enhanced to

ISSN (Online) 2620-7222
ISSN (Print) 2503-2399

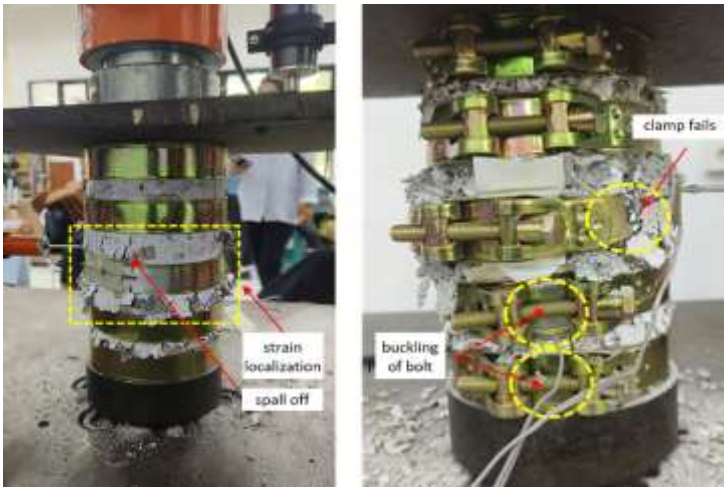

Source : (Experimental works, 2025).

Figure 8. Failure Modes of Confined Concrete Specimen.

nearly 25 MPa by the presence of external confinement by a steel clamp (strength enhancement ratio $\zeta = +2.33$). Similarly, the axial strain at peak load is also improved from 0.00107 to 0.00308 ($\zeta = +2.89$). The yield strain of the clamp $\varepsilon_{sy} = f_y/E_s = 0.000904$, is slightly lower than the yield strain of the unconfined concrete $\varepsilon_{cy} = 0.00107$. Hence, the steel clamp was in the yield state before the concrete cracks and successfully confined the concrete element, but had not failed until the concrete reached its peak stress. It can certainly be assumed that the stress and strain improvement can be more pronounced if the clear gap between each clamp unit is reduced. The displacement ductility μ_Δ of the confined column specimen was determined using the ratio of the yield displacement to the total displacement from the axial force versus the lateral displacement of the tested specimen provided in Figure 9(b). By the elasto-plastic approach, the yield displacement is 0.184 mm and the ultimate displacement is 0.982, resulting in the displacement ductility $\mu_\Delta = 5.77$. The displacement ductility relies upon the internal confinement by shear reinforcement [24] and external confinement as studied.

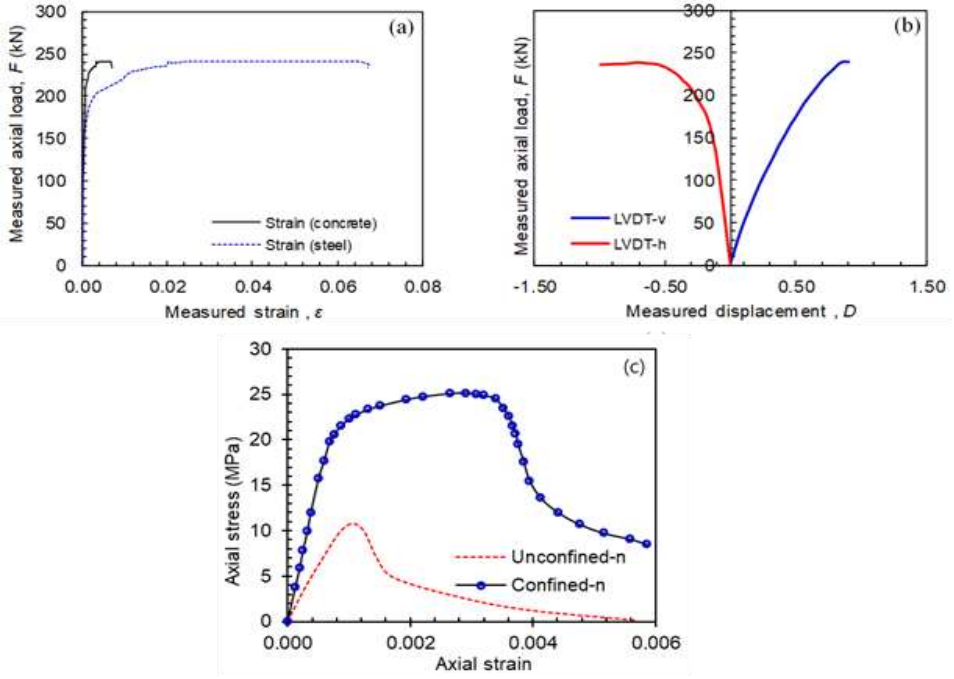

Source : (Experimental works, 2025).

Figure 9. Strain and Displacement Versus Axial Load Curves.

ISSN (Online) 2620-7222
ISSN (Print) 2503-2399

3.4. Confining Pressure Formulation

Confining pressure f_r suggested in [25] in Eqn. (1) was derived from the energy balanced method [26], where E_{frp} is the elastic modulus of FRP, t and $\varepsilon_{h,rup}$ represent the thickness and the rupture strain at hoop of FRP jacket, respectively. In contrast, the confining pressure in Eqn. (1) considers the full confinement method, whereas the clamp confinement approach of this study requires center-to-center spacing s_s between steel clamps that exhibits a major impact on the overall capacity. Moghaddam and Samandi [27] included the spacing in Eqn. (2), where $s_s = h_s + g_s$ as illustrated in Figure 10. A study [28] suggested k_s and k_h in Eqn. (3) and used k_s = 1 at the tie level for circular column section and neglected the reduction of concrete core area A_{co} by the area of longitudinal reinforcement in deriving k_h between tie level. This affects the compressive performance. Hence, Eqn. (4) takes into account the reduction. The placement of external confinement at the tie level and between tie levels also influences the pressure on to concrete surface. Figure 10 illustrates the confined and unconfined segments by ties and external confining steel.

$$f_r = \frac{2E_{frp}t\varepsilon_{h-rup}}{D} \tag{1}$$

$$f_r = \frac{2t_s f_y}{D}\frac{h_s}{h_s+g_s} \tag{2}$$

$$k_h = \left(1 - \frac{s\prime}{2d_s}\right)^2 \quad k_s = 1 - \frac{2(d_s-2r)^2}{3d_s^2} \quad \kappa_e = k_h k_s \tag{3}$$

$$k_h = \frac{A_{ce}}{A_{co}} = \frac{A_{co}-0.25\pi(d_s-s\prime/2)^2}{0.25\pi\left(d_s^2-n_b\phi^2\right)^2} = \frac{\left(1-\frac{s\prime}{2d_s}\right)^2}{\left(1-n_b\frac{\phi^2}{d_s}\right)^2} \tag{4}$$

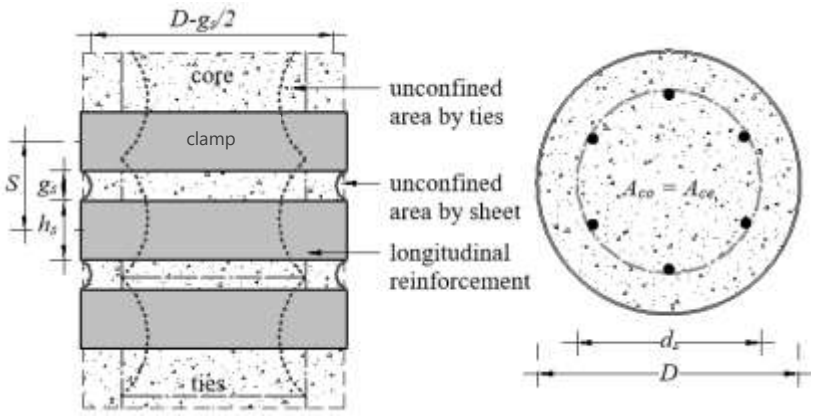

Source : (Analytical study, 2025).

Figure 10. Internal and External Confinement States.

In CFST [29], the increasing axial load application led to the lateral expansion of concrete core and steel sheets experiencing longitudinal stress σ_l, skin friction stress σ_z and hoop stress $\sigma_{\theta i}$. The outward expansion of the concrete causes the concrete core to experience triaxial stress called confining stress f_r. Although the skin friction stress σ_z between concrete surfaces and the steel clamps insignificantly affected the confining pressure in most cases, the analysis of this study includes σ_z to show the interaction between the interfaces. By the application of bolt tightening, an additional hoop stress $\sigma_{\theta b}$ is also considered, as shown in Figure 11(a), where σ_θ is the sum of $\sigma_{\theta i}$ and $\sigma_{\theta b}$. To compute all the stresses acting on the system, the

ISSN (Online) 2620-7222
ISSN (Print) 2503-2399

confining stress equations for a cylindrical concrete column confined by a steel clamp were derived from Von Mises failure criteria at yield in Eqn. (5) with the addition of the corresponding frictional stress during interface contact σ_z and κ_e. Assume $\sigma_z = 0$ at yield, the maximum value for σ_r and σ_θ is given in Eqn. (7) and Eqn. (8).

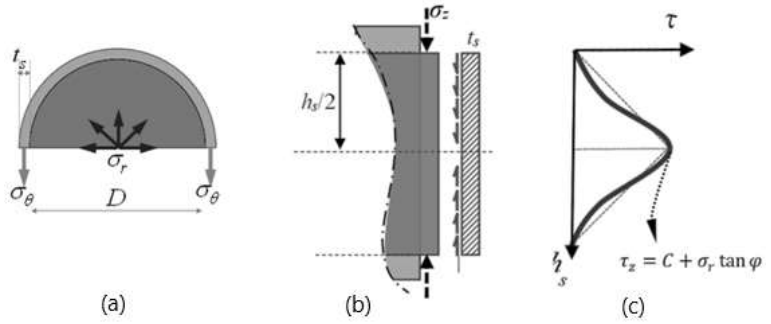

Source : (Analytical study, 2025).

Figure 11. Shear Friction Stress between Concrete and Steel Clamp.

$$f = \sigma_r^2 + \sigma_r^2 + \sigma_\theta^2 - \sigma_r\sigma_\theta - \sigma_\theta\sigma_z - \sigma_z\sigma_r = f_y^2 \quad (5)$$

$$\sigma_r = \frac{2(\varepsilon_\theta E_\theta)t_s h_s \kappa_e}{s_s D} \quad (6)$$

$$\sigma_r = \sqrt{f_y^2 - \sigma_\theta^2\left(1 - \frac{2t_s h_s \kappa_e}{s_s D}\right)} \quad (7)$$

$$\sigma_\theta = \sqrt{\frac{f_y^2 - \sigma_r^2}{\left(1 - \frac{2t_s h_s \kappa_e}{s_s D}\right)}} \quad (8)$$

The axial stress distribution is assumed to be linear up to the mid-height of the steel sheet. Once the slip occurred, the axial stress remains unchanged in the interface. Therefore, it is wise to average the axial stress along the height of the clamp as shown in Figure 11(c). The axial stress in the clamp can be defined by limiting the shear stress to its maximum condition as shown in Figure 11(c). When $\sigma_z \neq 0$, Mises' failure criterion can be rewritten as:

$$\left(1 - \frac{2t_s h_s \kappa_e}{s_s D}\right)\sigma_\theta^2 - \left(\sigma_z + \sigma_z \frac{2t_s h_s \kappa_e}{s_s D}\right)\sigma_\theta = f_y^2 - \sigma_r^2 - \sigma_z^2 \quad (9)$$

Providing $m = \frac{2t_s h_s \kappa_e}{s_s D}$, $A = (1 - m)$, $B = -(\sigma_z + \sigma_z m)$ and $C = -\left(f_y^2 - \sigma_r^2 - \sigma_z^2\right)$ yields a quadratic form that can be factorized for σ_θ and f_r. The validation of Eqn. (9) requires trials for consistent results of the confining pressure. For the current confined specimen, the confining pressure formula yields 9.28 MPa. The formula was also validated against relevant experimental results [13], [15], [30] as shown in Figure 12, for circular columns with the characteristic axial strength under 120 MPa. It is worth noting that the axial strength ratio of the confined concrete differs with the change of the characteristic compressive strength and the yield strength of the confining steel [18]. The regression analysis in Figure 12 shows that the axial strength of confined high-strength concrete (HSC) follows Eqn. (10), whereas that of confined normal strength concrete (NSC) follows Eqn. (11). Using the f_r value, the peak axial compressive strength of the strengthened specimen is 24.99 MPa, which perfectly fits the test result. It can be seen in the figure that the prediction of peak axial strength is more accurate at a lower f_r/f_c ratio of NSC and HSC. Both formulations can be further rewritten for the peak axial load.

$$f_{cc}/f_c = 3.32\frac{f_r}{f_c} + 1 \quad (10)$$

ISSN (Online) 2620-7222
ISSN (Print) 2503-2399

$$f_{cc}/f_c = 1.54\frac{f_r}{f_c} + 1 \quad (11)$$

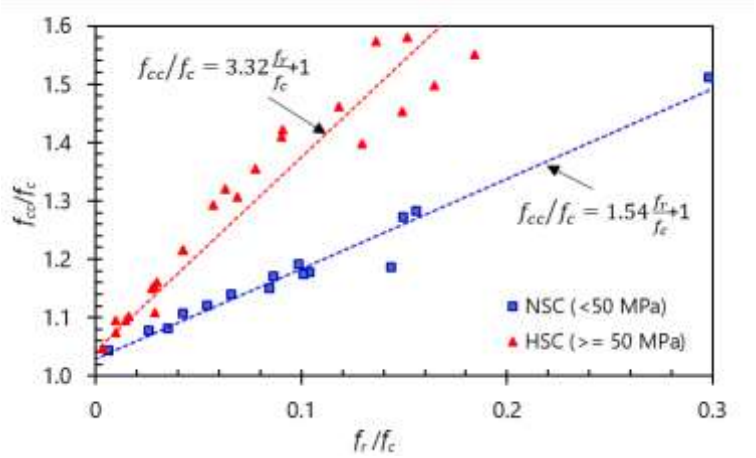

Source : (Analytical study, 2025).
Figure 12. Confining Pressure and Strength Ratio of NSC and HSC.

Researchers [16], [31] introduced the confinement factor η as the load ratio of the confining steel and concrete section in Eqn. (12) representing the confining steel sectional area A_s and the concrete sectional area A_c. This study uses a database comprising 52 experimental results shown in Figure 12 to obtain the correlation between η and f_{cc} as illustrated in Figure 13. Regression analysis yields the R^2 value of 96% indicating the strong relationship between the confining factor and f_{cc} by Eqn. (13). In contrast, the linear relationship only reaches 76% for HSC indicating that the relationship tends to be in quadratic form. Given that the axial stress of the confined concrete is determined using the conventional stress formula $f_{cc} = P_u/A_c$, then the ultimate axial load can be derived for the normal strength confined concrete using Eqn. (14). For the tested specimen, with η = 0.617, A_c = 9498.5 mm^2, the peak axial load using Eqn. (14) yields 240.22 kN, which is comparable to the test result.

$$\eta = \frac{A_s f_y}{A_c f_c} \quad (12)$$

$$f_{cc} = (2.21\eta + 1)f_c \quad (13)$$

$$P_u = (2.21\eta + 1)f_c A_c \quad (14)$$

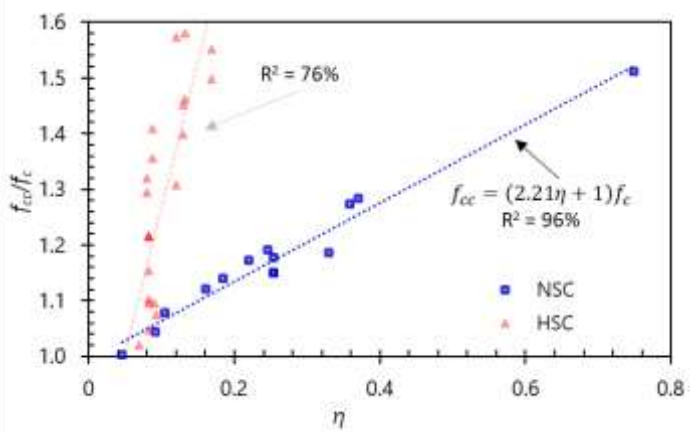

Source : (Analytical study, 2025).
Figure 13. Peak Confining Stress of NSC and HSC.

ISSN (Online) 2620-7222
ISSN (Print) 2503-2399

4. Conclusions and Suggestions

4.1 Conclusion

Cylindrical concrete columns with external confinement using a steel clamps have been investigated with concentric axial loading. Based on the test results and previous research data, the formulation of confining stress and peak axial load has been developed. Several conclusions can be drawn from the results of this study. External confinement using steel clamp increases the axial bearing capacity of concrete with a strength increase ratio of +2.33. The ultimate axial load increases from 101.67 kN to 241.4 kN (+2.37) and the ultimate axial deformation of concrete increases with a ratio of 2.89. Steel confinement clamps reach the yield state before concrete cracks and do not fail until the concrete reaches its ultimate strength. Vertical cracks, strain localization and cover spalling of the confined specimen are significantly reduced by the proposed confinement method since the internal stress of the concrete is evenly distributed along the height of the column. The proposed confining pressure and peak axial load formulations show a good fit to the experimental results of current and past studies.

4.2 Suggestion

Further studies should be conducted to consider the presence of opening gap that may degrade the actual axial strength and to develop the stress-strain model for the proposed confinement technique.

Acknowledgement

The first author would like to thank PPI Unika Atma Jaya Jakarta, the support of the Laboratory of Concrete, Advanced Materials and Computational Mechanics ITS Surabaya and Yayasan Pendidikan Tinggi Nusa Nipa.

References

[1] S. I. Yansiku, “Impact of artificially seismic loading on the response of building structure in various site classifications,” *J. King Saud Univ. - Eng. Sci.*, vol. 29, no. 4, pp. 302–312, 2017, doi: 10.1016/j.jksues.2017.06.002.

[2] J. Ji *et al.*, “Performance of concrete columns actively strengthened with hoop confinement: A state-of-the-art review,” *Structures*, vol. 54, pp. 461–477, 2023, doi: https://doi.org/10.1016/j.istruc.2023.05.038.

[3] N. Holmes, D. Niall, and C. O’Shea, “Active confinement of weakened concrete columns,” *Mater. Struct. Constr.*, vol. 48, no. 9, pp. 2759–2777, 2015, doi: 10.1617/s11527-014-0352-1.

[4] J. Červenka, V. Červenka, and S. Laserna, “On crack band model in finite element analysis of concrete fracture in engineering practice,” *Eng. Fract. Mech.*, vol. 197, no. April, pp. 27–47, 2018, doi: 10.1016/j.engfracmech.2018.04.010.

[5] S. I. Yansiku, “Characteristic of Concrete Containing Glass and Tyre Particles as Replacement of Fine Aggregate,” *Int. J. Adv. Sci. Eng. Inf. Technol.*, vol. 8, no. 4, p. 1055, Aug. 2018, doi: 10.18517/ijaseit.8.4.4274.

[6] S. I. Yansiku, “Karakteristik Kekuatan Beton Dengan Glass Powder, Fly Ash dan GBFS Sebagai Material Pengganti Semen,” *SIARTEK*, vol. 2, no. 2, p. 5, 2016.

[7] S. I. Yansiku, “Perilaku Kekuatan Beton Dengan Partikel Gelas Dan Karet Ban Bekas Sebagai Pengganti Pasir Alam,” *e-Jurnal Tek. Sipil dan Lingkung.*, vol. 2, no. 1, p. 10, 2018, [Online]. Available: http://jai.ipb.ac.id/index.php/jsil/article/view/15280

[8] X. Chen, Y. Yang, Y. Xue, and Y. Yu, “Behavior of axially and eccentrically loaded square RC columns retrofitted with steel strips,” *Case Stud. Constr. Mater.*, vol. 17, p. e01533, Dec. 2022, doi: 10.1016/J.CSCM.2022.E01533.

ISSN (Online) 2620-7222
ISSN (Print) 2503-2399

[9] L. H. Han, G. H. Yao, Z. P. Chen, and Q. Yu, "Experimental behavior of steel tube confined concrete (STCC) columns," *Steel Compos. Struct.*, vol. 5, no. 6, pp. 459–484, 2005.
[10] L. He, S. Lin, and H. Jiang, "Confinement effect of concrete-filled steel tube columns with infill concrete of different strength grades," *Front. Mater.*, vol. 6, Apr. 2019, doi: 10.3389/fmats.2019.00071.
[11] L. He, Y. Zhao, and S. Lin, "Experimental study on axially compressed circular CFST columns with improved confinement effect," *J. Constr. Steel Res.*, vol. 140, pp. 74–81, 2018, doi: 10.1016/j.jcsr.2017.10.025.
[12] H. Moghaddam, M. Samadi, K. Pilakoutas, and S. Mohebbi, "Axial compressive behavior of concrete actively confined by metal strips; part A: experimental study," *Mater. Struct.*, vol. 43, no. 10, pp. 1369–1381, 2010, doi: 10.1617/s11527-010-9588-6.
[13] A. Positong, T. Pannachet, and M. Boonpichetvong, "Discrete confinement by metal sheet strips on concrete columns under axial compression," *Int. J. GEOMATE*, vol. 15, no. 52, pp. 184–191, 2018, doi: 10.21660/2018.52.27093.
[14] J. Wei, Z. Xie, W. Zhang, X. Luo, Y. Yang, and B. Chen, "Experimental study on circular steel tube-confined reinforced UHPC columns under axial loading," *Eng. Struct.*, vol. 230, p. 111599, 2021, doi: https://doi.org/10.1016/j.engstruct.2020.111599.
[15] Y. Yang, Y. Xue, Y. Yu, and Y. Li, "Research on axial behaviour of concrete columns retrofitted with pre-stressed steel strips," *Mag. Concr. Res.*, vol. 72, no. 21, pp. 1089–1101, 2020, doi: 10.1680/jmacr.18.00107.
[16] Q. Yu, Z. Tao, W. Liu, and Z. B. Chen, "Analysis and calculations of steel tube confined concrete (STCC) stub columns," *J. Constr. Steel Res.*, vol. 66, no. 1, pp. 53–64, 2010.
[17] C. Zhou, X. Li, D. Wang, and S. Xia, "Analysis of bearing capacity and seismic performance of circular RC columns strengthened with externally wrapped steel plates," *Adv. Civ. Eng.*, vol. 2019, 2019, doi: 10.1155/2019/2515091.
[18] S. I. Yansiku, B. Piscesa, and P. Suprobo, "Numerical Study on Discrete Confinement of Circular RC Column Subjected to Eccentric Load," *Open Civ. Eng. J.*, vol. 17, 2023, doi: 10.2174/18741495-v17-e230917-2023-43.
[19] S. I. Yansiku, B. Piscesa, and P. Suprobo, "Numerical Study on Slender Circular Reinforced Concrete Column Clamped with Steel Sheet," *IOP Conf. Ser. Earth Environ. Sci.*, vol. 1244, no. 1, 2023, doi: 10.1088/1755-1315/1244/1/012002.
[20] BSN, *SNI 03-2834-1993: Tata Cara Pembuatan Campuran Beton Normal*. Jakarta, Indonesia: Departemen Pemukiman dan Prasarana Wilayah, 1993.
[21] C. Wu and C. K. Y. Leung, "Strain-Hardening Cement-Based Composites," in *SHCC: International Conference on Strain-Hardening Cement-Based Composites*, V. Mechtcherine, V. Slowik, and P. Kabele, Eds., Germany: Springer Dordrecht, 2017, pp. 28–36. doi: https://doi.org/10.1007/978-94-024-1194-2.
[22] R. Park and T. Paulay, *Reinforced Concrete Structure*. Toronto, Canada: John Wiley & Sons Inc., 1975.
[23] A. Maysyurah, A. Rusdi, and A. Didik Setyo Purwantoro, "Compressive Strength Of Concrete The Time Setting Of Application Of Plastiment® P-121 Additive Mixture," *Civilla J. Tek. Sipil Univ. Islam Lamongan*, vol. 9, no. 1 SE-Jurnal CIVILA, pp. 39–46, Mar. 2024, doi: 10.30736/cvl.v9i1.1185.
[24] Aldivonso Tambunan and S. A. R. S. Hasibuan, "Study on the Ductility Behavior of Reinforced Concrete Columns with 10 mm Shear Reinforcement Diameter under Variable Axial Loads," *Civilla J. Tek. Sipil Univ. Islam Lamongan*, vol. 10, no. 1 SE-Jurnal CIVILA, pp. 101–112, Apr. 2025, doi: 10.30736/cvl.v10i1.1410.
[25] T. Jiang and J. G. Teng, "Analysis-oriented stress–strain models for FRP–confined

ISSN (Online) 2620-7222
ISSN (Print) 2503-2399

concrete," *Eng. Struct.*, vol. 29, no. 11, pp. 2968–2986, 2007, doi: https://doi.org/10.1016/j.engstruct.2007.01.010.

[26] F. E. Richart, A. Brandtzaeg, and R. L. Brown, "A Study of the Failure of Concrete under Combined Compressive Stresses," Illinois, USA, 1928.

[27] H. Moghaddam, M. Samadi, and K. Pilakoutas, "Compressive behavior of concrete actively confined by metal strips, part B: analysis," *Mater. Struct.*, vol. 43, no. 10, pp. 1383–1396, 2010, doi: 10.1617/s11527-010-9589-5.

[28] S. Sheikh and S. M. Uzumeri, "Analytical Model for Concrete Confinement in Tied Columns," *J. Struct. Div.*, vol. 108, pp. 2703–2722, Dec. 1982, doi: 10.1061/JSDEAG.0006100.

[29] A. H. Yudhanto, B. Piscesa, M. M. Attard, B. Suswanto, and P. Suprobo, "Finite element modeling of concrete confined with circular thin-walled steel sheet," *E3S Web Conf.*, vol. 156, pp. 0–5, 2020, doi: 10.1051/e3sconf/202015605009.

[30] J. Liu, Y. Teng, Y. Zhang, X. Wang, and Y. F. Chen, "Axial stress-strain behavior of high-strength concrete confined by circular thin-walled steel tubes," *Constr. Build. Mater.*, vol. 177, pp. 366–377, 2018, doi: 10.1016/j.conbuildmat.2018.05.021.

[31] L. H. Han, "Experimental behaviors of steel tube confined concrete (STCC) columns," *Steel Compos. Struct.*, vol. 5, no. 6, pp. 459–484, 2005.